Incorporation of a deformation prior in image reconstruction

Barbara Gris *

Abstract

This article presents a method to incorporate a deformation prior in image reconstruction via the formalism of deformation modules. The framework of deformation modules allows to build diffeomorphic deformations that satisfy a given structure. The idea is to register a template image against the indirectly observed data via a modular deformation, incorporating this way the deformation prior in the reconstruction method. We show that this is a well-defined regularization method (proving existence, stability and convergence) and present numerical examples of reconstruction from 2-D tomographic simulations and partially-observed images.

1 Introduction

For many imaging techniques, the acquisition time is relatively long. For instance in computed tomography targeting the torso, the acquisition takes several minutes and then the patient breathes during the acquisition. Using static reconstruction methods leads to the appearance of motion artefacts which can prevent from identifying some structures or, on the contrary, creates false ones. The solution that is used in clinic for torso computed tomography is to use "gated data": the respiratory rhythm of the patient is recorded simultaneously, and only the data acquired at a specific respiratory state are used for the reconstruction. In order to be able to use all the available data, it is necessary to incorporate a temporal component in the reconstruction method [23, 25, 26, 35].

In order to do so, a common strategy [2, 11, 13, 14, 15, 21, 22, 27, 33, 34, 40] is to reconstruct one initial image I_0 and a trajectory of deformations $t \mapsto \varphi_t = \varphi(t, \cdot)$ such that for each time t the image $\varphi_t \cdot I_0$ (deformation of I_0 by φ_t) matches the observed data. Then the framework has two intertwined components, estimation of I_0 and estimation of $t \mapsto \varphi_t$, that can be alternatively performed in an iterative optimization scheme. This article concentrates on the second step: estimating the deformation trajectory $t \mapsto \varphi_t$, given observed data and an initial template image I_0. A central point is to define the deformation model, *i.e.* the set of deformations that are considered and their parametrization. In [14] and [22] for instance, the deformation model is built via the LDDMM (Large Deformation Metric mapping) framework [8], leading to good numerical and theoretical results. However, as illustrated in the following, this deformation model corresponds to *unstructured deformations* in the sense that it is not possible to incorporate a prior knowledge about the type of deformations that can occur (see Section 2.3). As a consequence, in some cases the estimated deformation is not intuitively satisfying but there is no possibility with such an unstructured-deformation framework to enforce a more intuitive solution. Several frameworks allow to incorporate particular priors in deformation models [7, 6, 16, 28, 32, 36, 37, 38, 42] so that they are adapted to specific situations. The goal of this article is to show how a generic prior on the set of deformations can be incorporated

*LJLL - Laboratoire Jacques-Louis Lions, UPMC, Paris, France.

via the notion of deformation modules [18] so that only the desired solutions are used to reconstruct an image from the observed data and the initial template. For instance in the case of biological images, this framework would ensure that only the deformations that are possible from a biological point of view are considered. The interest of the deformation module framework is that it encompasses many previous approaches and requires very few conditions on the constraints that can be incorporated in the deformation model.

We recall the notion of deformation modules and build a particular class of deformation modules called *constrained translations generator (CTG) deformation modules* that can be easily built and used. We present how geodesic trajectories can be used to reconstruct an image from indirect observations and a given initial template, and then we show that this strategy is a well-defined regularization method to solve inverse problems by proving the existence of solutions as well as their stability and convergence. Finally we present several numerical examples, using our framework to reconstruct images from 2-D simulations of two different natures: tomographic data (obtained via the 2-D Radon transform) and partial observation (obtained by restricting the image on a small window).

2 Background

2.1 Inverse problem

Let $\Omega \subset \mathbb{R}^n$ be a fixed open bounded domain (with $n = 2$ or 3) and $X := L^2(\Omega, \mathbb{R})$ be a space of grey scale images on Ω. The principle of inverse problem is to reconstruct an image $I \in X$ from an indirect observation $d \in Y$ the data space. More precisely, we suppose that there is a ground truth image I_{truth} in X and an operator $T : X \mapsto Y$ such that the observed data is $d = T(I_{truth}) + \epsilon$ where ϵ is some noise. The goal is to build an image I such that $T(I)$ approaches d, *i.e.* to minimize the quantity $D\Big(T(I), d\Big)$ (where D is a distance on the data space Y). In general there is not a unique image I minimizing it and a general strategy is to define a regularity function $R : X \mapsto \mathbb{R}_{\geq 0}$ and then to minimize $I \in X \mapsto D\Big(T(I), d\Big) + R(I)$.

2.2 Inverse problem with an image prior

If a reference image I_0 is known to be close (in a certain sense to specify) to the image to reconstruct, this prior knowledge can be incorporated in the reconstruction by defining a regularity function R that depends on the reference image I_0. A first idea is to consider $R(I) = |I - I_0|_X^2$ where $|\cdot|_X$ is the L^2-norm. However this norm might not be appropriate as it depends on point-wise comparison of images: in section 5 we show an example where this regularization is not satisfying. In [1, 9, 24], the authors use the mass-transport penalization between I and I_0. This approach leads to good numerical results but assumes that the grey-level on images can be modelled as a mass: the penalization of the displacement of a given area depends on its grey-scale value, which is not necessarily relevant in practice. Other frameworks, as developed for instance in [14, 22, 31], consist in defining the regularity function R on a space of deformations so that the functional to minimize is $\varphi \mapsto D\Big(T(\varphi \cdot I_0), d\Big) + R(\varphi)$ where φ stands for a deformation. These frameworks are based on the idea of image registration. Various theoretical and numerical frameworks were developed in order to perform image registration [8, 10, 20, 29, 41]. The one used in [14, 22, 31] is the Large Deformation Metric Mapping one (LDDMM, see [8, 41]) where deformations are diffeomorphisms built from vector fields. Following [31] we will denote such approaches by *indirect registration*. As this approach is close to the one that we propose in the following, we detail it in the next section. The main idea here (in opposition to the mass transport framework) is that the image I can be seen as a *geometric transformation* of the reference image I_0: it can for instance be relevant in the case of the motion of a patient. The framework that we propose is based on this idea but uses an additional prior on the *nature of the motion*: we will suppose that there are known constraints on the possible motions and we incorporate them in the reconstruction method via the notion of deformation modules.

2.3 Large deformations and indirect registration

We detail here the framework of indirect registration with large deformations as developed in [14, 22]. Let us define the group $\mathrm{Diff}_0^\ell(\Omega)$ of C^ℓ-diffeomorphisms that tend to Identity at the boundary of Ω. It is an open set of $Id + C_0^\ell(\Omega, \mathbb{R}^n)$ where $C_0^\ell(\Omega, \mathbb{R}^n)$ is the space of vector fields ℓ times continuously differentiable, supported on Ω, with derivatives tending to zero at the boundary. It is equipped with the norm $|v|_\ell = \sup\{|\frac{\partial^{\ell_1+\cdots+\ell_d} v(x)}{\partial x_1^{\ell_1}\ldots x_d^{\ell_d}}| \mid x \in \mathbb{R}^d, (\ell_1, \ldots, \ell_d) \in \mathbb{N}^d, \ell_1 + \cdots + \ell_d \leq \ell\}$ such that it is a Banach space. It is necessary to define how these diffeomorphisms can transform an image. There are several possible choices, in the following we will consider the *geometric group action* of diffeomorphisms on X defined by $\varphi \cdot I = I \circ \varphi^{-1}$ for $\varphi \in \mathrm{Diff}_0^\ell(\Omega)$ and $I \in X$.

The deformations that we will consider are *large deformations* defined as flows of a time-varying vector-field:

Proposition 1. *[3] Let V be a fixed Hilbert space of vector fields on Ω continuously embedded in $C_0^\ell(\Omega, \mathbb{R}^n)$ and let $v \in L^2([0,1], V)$. Then the following ordinary differential equation*

$$\begin{cases} \dfrac{\partial}{\partial t}\varphi_t(x) = v\big(t, \varphi_t(x)\big) \\ \varphi_{t=0} = Id \end{cases} \qquad \text{for any } x \in \Omega \text{ and } t \in [0,1]. \tag{1}$$

has a unique absolutely continuous solution and it is a diffeomorphism at each time. It is called the flow of v *and we will denote it by $\varphi_t^v \in \mathrm{Diff}_0^\ell(\Omega)$.*

In this context, the strategy of indirect registration of a template image $I_0 \in X$ against some data $d \in Y$ is then to minimize a functional of the form

$$J\colon v \in L^2([0,1], V) \mapsto C(v) + \frac{1}{\lambda} D\Big(T(\varphi_{t=1}^v \cdot I_0), d\Big)$$

where D is a distance on Y, $C\colon L^2([0,1], V) \mapsto \mathbb{R}_{\geq 0}$ is continuous and $\lambda > 0$.

This framework leads to good result (see [14] and also [22] where the LDDMM registration was adapted to 4D reconstruction) but sometimes the obtained deformation, and hence the reconstructed image, are not intuitively satisfying. For instance we present in Figure 1 the result of the indirect registration of the template image presented in Figure 1a against the data d presented in Figure 1b which are the Ray transform with 100 angles uniformly distributed in $[0, \pi]$ of the ground truth image Figure 1c. Even though the reconstructed image in Figure 1h is not too far (for the L^2 metric for instance) from the ground truth image, intuitively it would have been more satisfying to obtain a deformation rotating the small white structure than one distorting it like here. In particular when keeping in mind the goal of modelling (patients) motions. It would be interesting to force the deformation to be a local rotation, and then to optimise the parameters of this rotation. With this *non structured* indirect matching, it is only possible to choose

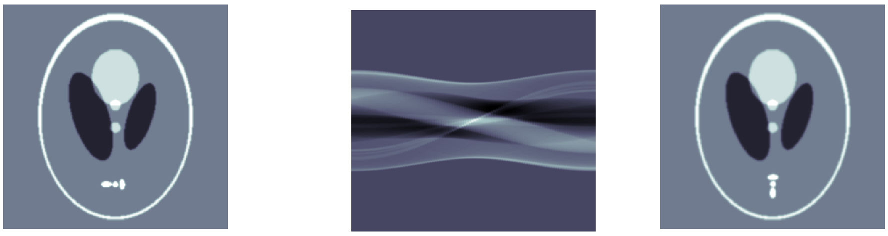

(a) Template.

(b) Data.

(c) Ground truth.

(d) $t = 0$.

(e) $t = 0.25$.

(f) $t = 0.5$.

(g) $t = 0.75$.

(h) $t = 1$.

Figure 1: Result of LDDMM-based indirect matching. Template I_0 in Figure 1a matched against data d in Figure 1b obtained from ground truth in Figure 1c (forward operator: Ray transform with 100 angles uniformly distributed in $[0, \pi]$). Second row: image trajectory $\varphi_t^v \cdot I_0$, the reconstructed image is in Figure 1h.

the fixed space of vector fields V but not to incorporate the additional knowledge of the type of transformation that we would like to observe. As specified in the introduction, several frameworks [6, 7, 16, 28, 32, 36, 37, 38, 42] allow to build particular structured deformation models that are adapted to specific situations. However they do not provide a generic framework for structured deformations and, to our knowledge, were not adapted to image reconstruction.

Remark 1. *This diffeomorphic approach (as well as the one that we develop in the following) supposes that the image I can be modelled as the deformation of the reference image I_0. The transformation of an image by a diffeomorphism can be defined, like here, via the geometric group action $(\varphi, I) \mapsto I \circ \varphi^{-1}$ so that the new transformed image has the same level sets as the original one. It is also possible to use a* mass-preserving *action $(\varphi, I) \mapsto |D\varphi^{-1}| I \circ \varphi^{-1}$ where the level sets can change but where the mass is preserved. With the latter action, it is possible to reconstruct an image I with grey-scale values that are different from the reference image I_0 but these changes are due to a change of volume in the deformation (via the term $|D\varphi^{-1}|$). With this diffeomorphic model it is therefore not possible to reconstruct an image I as a transformation of a reference image I_0 if the grey-scale values of I_0 are not correct (for instance if the background does not have the correct value or if there is a new structure in I). This issue has been adressed using the metamorphosis framework [39] (allowing a change in the grey-scale value in addition to the diffeomorphic deformation) in [19] with an ODE formulation (following the idea of indirect registration of [14]) and in [30] with a PDE formulation that is solved using a time discrete path method.*

3 Deformation modules

The object of this article is to show how the framework of *deformation modules* introduced in [18] can be used to incorporate motion prior in image reconstruction via a *constrained* indirect registration. The first step is to build *constrained vector fields* in Section 3.1 and then *constrained large deformations* in Sections 3.4 and 3.5.

3.1 Definition

The intuition behind the deformation module framework is to constrain deformations in order to incorporate some prior in the motion, while leaving some parameters free in order to be able to adapt to data. For instance if the goal is to reconstruct a respiratory motion, even though this motion is different from one patient to another, there might be some shared "base-motions" from which any respiratory motion can be reconstructed. These "base-motions" can be modelled by some generators that, given the current "geometrical state" of the subject, would define a family of vector fields which can then be combined to produce the respiratory motion. The current "geometrical state" of the subject can be given via its image or some other geometrical variable such as landmarks, and the coefficients of the combination of the vector fields correspond to a "control variable" in the sense that they have to be optimized so that the global motion fits to the data. The framework of deformation modules formalizes this intuition. The idea of "geometrical state" is formalized by the notion of "shape" defined by S. Arguillere in [4], we give here the simplified version of this notion that we will use:

Definition 1. *Let m be an integer, $\mathcal{O}$ be an open subset of $\mathbb{R}^m$ and $k > 0$ a non-negative integer. Assume that the group $\mathrm{Diff}_0^\ell(\Omega)$ acts continuously on $\mathcal{O}$, according to the action*

$$\begin{array}{rcl} \mathrm{Diff}_0^\ell(\Omega) \times \mathcal{O} & \to & \mathcal{O} \\ (\phi, o) & \mapsto & \phi \cdot o\,. \end{array} \tag{2}$$

*We say that $\mathcal{O}$ is a C^k-**shape space of order** ℓ on Ω if the following conditions are satisfied:*

1. *For each $o \in \mathcal{O}$, $\phi \in \mathrm{Diff}_0^\ell(\Omega) \mapsto \phi \cdot o$ is Lipschitz with respect to the norm $|\cdot|_\ell$ and is differentiable at Id_Ω. This differential is called the **infinitesimal action** of $C_0^\ell(\Omega)$ and we will simply denote the action of a vector field v on a shape o (with a slight abuse of notation) by $v \cdot o$.*

2. *The mapping $(o, v) \in \mathcal{O} \times C_0^\ell(\Omega) \mapsto v \cdot o$ is continuous and its restriction to $\mathcal{O} \times C_0^{\ell+k}(\Omega)$ is of class C^k.*

*An element o of $\mathcal{O}$ is called a **shape**, and $\mathbb{R}^n$ will be referred to as the **ambient space**.*

We will use this notion of shape in order to formalize the intuition of "geometrical state" introduced previously. The notion of deformation modules that we will present now formalizes the intuition of "base motions" associated to a geometrical state. These base motions form a (small) subset of the space of vector fields $C_0^\ell(\Omega, \mathbb{R}^n)$ that can act on the shape space.

We give a slightly simplified formal definition of a deformation module from the one defined in [18]:

Definition 2. *Let $k, \ell \in \mathbb{N}^*$. We say that $M = (\mathcal{O}, H, \zeta, c)$ is a C^k-**deformation module of order** ℓ with **geometrical descriptors** in $\mathcal{O}$, **controls** in H, **field generator** ζ and **cost** c, if*

- *$\mathcal{O} \subset \mathbb{R}^m$ is a C^k-shape space on Ω of order ℓ with an infinitesimal action $C_0^\ell(\Omega) \times \mathcal{O} \longrightarrow \mathbb{R}^m$,*
- *H is a finite-dimensional Euclidean space,*
- *$\zeta\colon (o, h) \in \mathcal{O} \times H \to \zeta_o(h) \in C_0^\ell(\Omega, \mathbb{R}^n)$ is continuous, with $h \mapsto \zeta_o(h)$ linear and $o \mapsto \zeta_o$ of class C^k,*
- *$c\colon (o, h) \in \mathcal{O} \times H \to c_o(h) \in \mathbb{R}^+$ is a continuous mapping such that $o \mapsto c_o$ is smooth and for all $o \in \mathcal{O}$, $h \mapsto c_o(h)$ is a positive quadratic form on H, thus defining a smooth metric on $\mathcal{O} \times H$.*

The field generator ζ plays the role of generator of the "base-motions", it takes as input couples of a geometrical descriptor and a control variable. The geometrical descriptor is the variable giving some geometrical information and leading to the specification of the constraints (for instance specifying the location of the generated vector field). The control variable specifies how to combine these constraints. As the geometrical descriptor corresponds to "geometric information", if the geometry of the ambient space is modified through a deformation, the geometrical descriptor should be transformed accordingly. This is why it is necessary to specify how vector fields can act on geometrical descriptors via the infinitesimal action of the shape space $\mathcal{O}$. The importance of this parameter will be detailed with the definition of modular large deformations in Section 3.4.

Remark 2. *In [18], the deformation module was defined by a five-fold $(\mathcal{O}, H, \zeta, \xi, c)$ where ξ is the infinitesimal action associated to the shape space $\mathcal{O}$. Here in order to simplify the notations (and as in the examples we present there is no ambiguity about them), we will denote all the infinitesimal actions by $v \cdot o$ and they will be implicitly defined via the shape spaces of geometrical descriptors.*

In the following we will restrict ourselves to deformation modules satisfying the Uniform Embedding Condition:

Definition 3. *Let $M = (\mathcal{O}, H, \zeta, c)$ be a C^k-deformation module of order ℓ. We say that M satisfies the* ***Uniform Embedding Condition (UEC)*** *if there exists a Hilbert space of vector fields V continuously embedded in $C_0^{\ell+k}(\Omega)$ and a constant $\gamma > 0$ such that for all $o \in \mathcal{O}$ and for all $h \in H$, $\zeta_o(h) \in V$ and*

$$|\zeta_o(h)|_V^2 \leq \gamma c_o(h)\,.$$

This condition will be required for the theoretical results presented in the following sections. In the following we will use particular Hilbert spaces that are called Reproducing Kernel Hilbert Space (RKHS) (see for instance [5]):

Definition 4. *Let $(V, \langle \cdot, \cdot \rangle_V)$ be a Hilbert space of functions $\Omega \mapsto \mathbb{R}^n$. We say that V is a Reproducing Kernel Hilbert Space (RKHS) if for each $x \in \Omega$, $\delta_x\colon f \in H \mapsto f(x) \in \mathbb{R}^n$ is continuous.*

If $(V, \langle \cdot, \cdot \rangle_V)$ is a RKHS, then for each $(x, \alpha) \in \Omega \times \mathbb{R}^n$, the function $\delta_x^\alpha\colon f \in V \mapsto (\alpha, f(x))_{\mathbb{R}^n}$ belongs to V^* (space of continuous linear forms on V) and, from the Riesz theorem, we can define the reproducing kernel of V:

Proposition 2. *Let $(V, \langle \cdot, \cdot \rangle_V)$ be a RKHS, there exists a unique operator $K_V\colon V^* \mapsto V$ such that for all $(f, h) \in V \times V^*$, $(h, f) = \langle K_V h, f \rangle_V$. Besides, for each $(x, y) \in \Omega^2$, there exists a unique matrix $K(x, y)$ such that for all $(\alpha, \beta) \in \mathbb{R}^n \times \mathbb{R}^n$, $\alpha^T K(x, y)\beta = \langle K_V \delta_x^\alpha, K_V \delta_y^\beta \rangle_V$.*

It can be shown (see [5]) that the RKHS V can be totally defined from the function $K\colon (x,y) \mapsto K(x,y)$ and in the following we will use *scalar Gaussian RKHS* which are defined from a function $K\colon (x,y) \mapsto K_\sigma(x,y)I_n$ where I_n is the identity matrix of $\mathbb{R}^n$, $\sigma \in \mathbb{R}$ and $K_\sigma\colon (x,y) \mapsto \exp\Big(-\frac{|x-y|^2}{2\sigma^2}\Big) \in \mathbb{R}$. These RKHS are then defined by their *scale* σ.

3.2 Examples

We will now present some examples that are very simple to define and that will simultaneously be very useful in the following. They all satisfy the uniform embedding condition. All the images are defined on $\Omega =]-16,16[\times]-16,16[$ which is discretized in 256×256 pixels.

3.2.1 Local translations

Let us consider again the image in Figure 1a and imagine that there is a prior on the way it can be transformed. Suppose that we know that there are two forces that can push or pull in any direction, acting in areas of given sizes. A way to model these forces is by using local translations. Then let us build a deformation module generating vector fields that are always a sum of two local translations, localized via a scalar Gaussian kernel $K_\sigma\colon (x,y) \mapsto \exp -\frac{|x-y|^2}{2\sigma^2}$ (we fix the kernel size σ, see Section 3.1). The generated vector fields will then be parametrized by:

- 2 points, centres of the local translations: they define the locations of the translations given the current geometrical state and then are geometrical descriptors
- 2 vectors, vectors of the local translations: they define how the two local translations can be used to generate an adapted vector field and then they are control variables.

The space of geometrical descriptors is therefore $\mathcal{O} = \Omega \times \Omega$ (space of two points), the space of controls is $H = \mathbb{R}^2 \times \mathbb{R}^2$ (space of two vectors) and the field generator is $\zeta\colon (o,h) \in \mathcal{O} \times H \mapsto \sum_{i=1}^2 K_\sigma(o_i,\cdot)h_i$ with $o = (o_1,o_2)$ and $h = (h_1,h_2)$. A natural choice for the infinitesimal action of $\mathcal{O}$ is the application of vector fields to the two points: $(o,v) \in \mathcal{O} \times C_0^\ell(\Omega,\mathbb{R}^2) \mapsto v \cdot o = (v(o_1),v(o_2))$ with $o = (o_1,o_2)$. The cost can be chosen as $c\colon (o,h) \mapsto |\zeta_o(h)|^2_{V_\sigma}$ with V_σ the RKHS associated with K_σ so that the defined deformation module $M = (\mathcal{O},H,\zeta,c)$ straightforwardly satisfies the UEC. The set of vector fields that can be generated by this deformation module is rich, as illustrated in Figure 2, but these vector fields follow the strong prior of being sums of two local translations.

3.2.2 Contracting-dilating field

Suppose now that one has an additional prior on the directions of the vectors of the two translations: that they should both be parallel to the line between the two centres and in opposite direction. In this case it is not adapted to let the vectors of the translation being controls variables as they cannot be chosen freely. On the contrary the directions are now a function of the geometrical descriptor, and the variable that can now be freely chosen is a scalar to which will be multiplied the vectors of the translations. More precisely we can set, for this new deformation module, $\tilde{\mathcal{O}} = \Omega \times \Omega$, $\tilde{H} = \mathbb{R}$ and $\tilde{\zeta}\colon (o,h) \in \tilde{\mathcal{O}} \times \tilde{H} \mapsto h\Big(K(o_1,\cdot) - K(o_2,\cdot)\Big)(o_1 - o_2)$ with $o = (o_1,o_2)$. We define as previously, the infinitesimal action of $\tilde{\mathcal{O}}$ by $(o,v) \in \tilde{\mathcal{O}} \times C_0^\ell(\Omega,\mathbb{R}^2) \mapsto v \cdot o = (v(o_1),v(o_2))$ and $\tilde{c}\colon (o,h) \mapsto |\zeta_o(h)|^2_{V_\sigma}$. We present in Figure 3 several examples of vector fields generated by this deformation module

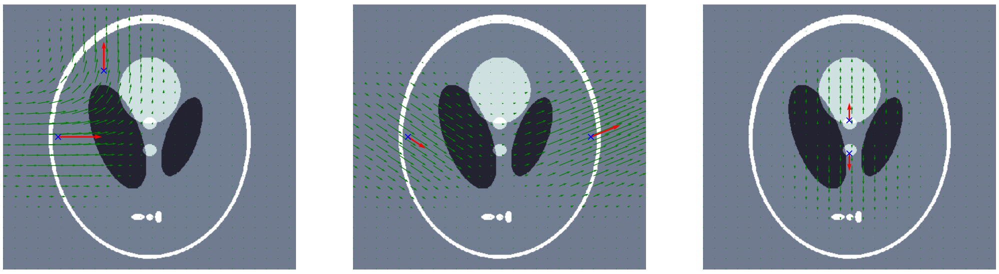

Figure 2: Three examples of vector field generated by a deformation module generating sums of two local translations (see Section 3.2.1, $\sigma = 6$) for three different values of geometrical descriptors and controls. The blue crosses are the geometrical descriptors, the red arrows are the controls and the vector fields are plotted in green.

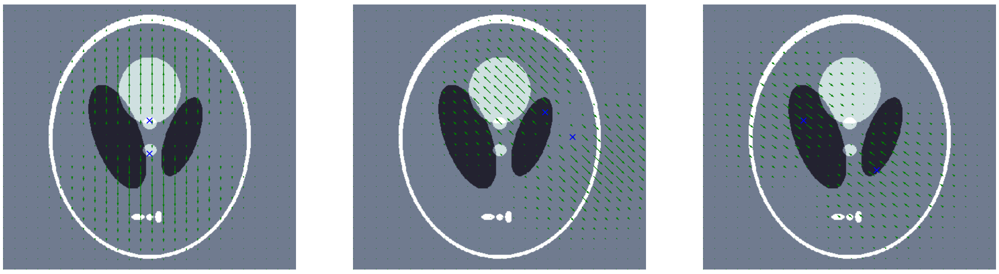

Figure 3: Three examples of vector field generated by a deformation module generating contracting or dilating field (see Section 3.2.2, $\sigma = 8$) for three different values of geometrical descriptors and controls. The blue crosses are the geometrical descriptors, the vector fields are plotted in green. The scalar control is positive for the left and middle figure, and negative for the figure on the right.

$\tilde{M} = (\tilde{\mathcal{O}}, \tilde{H}, \tilde{\zeta}, \tilde{c})$. Note that the vector fields generated by $\tilde{M}$ can also be generated by M but that they are not parametrized in the same manner: an additional prior comes with $\tilde{M}$.

3.2.3 Constrained translations generator (CTG) deformation modules

In the following we will use a certain category of deformation modules that generate vector fields which are a constrained sum of local translations, generalizing the ones previously presented in Section 3.2.2. More precisely we set a scale $\sigma \in \mathbb{R}_{>0}$, $N \in \mathbb{N}$ and two functions $f\colon (\mathbb{R}^n)^N \mapsto (\mathbb{R}^n)^p$ (a *point-generator function*) and $g\colon (\mathbb{R}^n)^N \mapsto (\mathbb{R}^n)^p$ (a *vector-generator function*) with $p \in \mathbb{N}$. Then we define $\mathcal{O} = \Omega^N$ (space of N points), $H = \mathbb{R}$ and $\zeta\colon (o, h) \in \mathcal{O} \times H \mapsto h \sum_{i=1}^{p} K_\sigma(f_i(o), \cdot) g_i(o)$ with $f = (f_i)$ and $g = (g_i)$, where K_σ is the scalar Gaussian kernel of size σ (see Section 3.2.1).

The idea here is to associate, to each geometrical descriptor o, a set of points - $(f_1(o), \dots, f_p(o))$ and a set of vectors $(g_1(o), \dots, g_p(o))$ so that the vector fields that can be generated with o are colinear to the sum of the local translations centred at points $f_i(o)$ with vectors $g_i(o)$. The infinitesimal action can be simply defined by the application of the vector field to the points composing the geometrical descriptor and the cost by $c\colon (o, h) \in \mathcal{O} \times H \mapsto \epsilon |\zeta_o(h)|^2_{V_\sigma} + h^2$ for some $C > 0$. This definition as a sum of these two terms is due to regularity reasons, ensuring that c_o is a quadratic form on H for all o in $\mathcal{O}$

and that the deformation module satisfies the uniform embedding condition. Deformation modules that can be defined this way will be called *constrained translations generator deformation modules* and refered to as *CTG modules.*

Remark 3. *In the following we will only use scalar Gaussian kernels, so we will only specify the scale σ in order to define the used kernel. This kernel is smooth and then the generated vector fields are also smooth. As a consequence, constrained translations generator deformation modules are C^k-deformation modules of order ℓ for any $k, \ell \geq 1$ such that f and g are C^k.*

These deformation modules are defined by three parameters: the kernel-size σ, the point-generator function f and the vector-generator function g. We present in Figure 4 various vector fields generated by various deformation modules, *i.e.* for various choices of σ, f and g.

3.3 Combining deformation modules

An interesting feature of this framework is that deformation modules can be combined to form a compound deformation module that will generate vector fields that are a sum of the vector fields generated by the combined deformation modules. More precisely:

Definition 5. *Let $M^l = (\mathcal{O}^l, H^l, \zeta^l, c^l)$, $l = 1 \dots L$, be L C^k-deformation modules of order ℓ. We define the* ***compound module*** *of modules M^l by $\mathcal{C}(M^l, l = 1 \dots L) = (\mathcal{O}, H, \zeta, \xi, c)$ where $\mathcal{O} = \prod_l \mathcal{O}^l$, $H = \prod_l H^l$ and for $o = (o^l)_l \in \mathcal{O}$, $\zeta_o \colon h = (h^l) \in H \mapsto \sum_l \zeta^l_{o^l}(h^l)$, $v \cdot o = (v \cdot o^l)_l \in T_o\mathcal{O}$ (for $v \in C_0^\ell(\mathbb{R}^n)$) and $c_o \colon h = (h^l) \in H \mapsto \sum_l c^l_{o^l}(h^l)$.*

As shown in [18], the uniform embedding condition is stable under combination and then an easy way to build complex deformation modules satisfying the uniform embedding condition is to combine several simple deformation modules satisfying this condition.

In Figure 5 we present three examples of vector fields generated by two different compound deformation modules.

In the following we will consider deformation modules $M = (\mathcal{O}, H, \zeta, c)$ that are obtained through combination of CTG modules. The space of geometrical descriptors $\mathcal{O}$ is then made of points of the ambient space $\mathbb{R}^n$ so there exists $m \in \mathbb{N}$ such that $\mathcal{O} \subset (\mathbb{R}^n)^m$. As a consequence, when necessary, we will specify this number of points m.

Remark 4. *If $M = (\mathcal{O}, H, \zeta, c)$ is obtained through combination of CTG modules such that ζ is C^k, then M is a C^k-deformation module of order ℓ for any $\ell > 0$.*

3.4 Modular large deformations

The notion of deformation module allows to constrain *vector fields* via the field generator ζ. The next step in order to define a *constrained indirect registration* consists in specifying how deformation modules can be used to build *large deformations* so that the constraints on vector fields are transformed into constraints on diffeomorphisms. Large deformations are obtained as flows of time-varying vector fields and the idea is then to consider only vector fields that can be generated by the field generator of a given deformation module. These trajectories of vector fields are then parametrized by trajectories of geometrical descriptors and controls and then in order to defined *modular large deformations*, one needs to specify the trajectories of geometrical descriptors and controls that will be considered. We will consider what we call *controlled path of finite energy*:

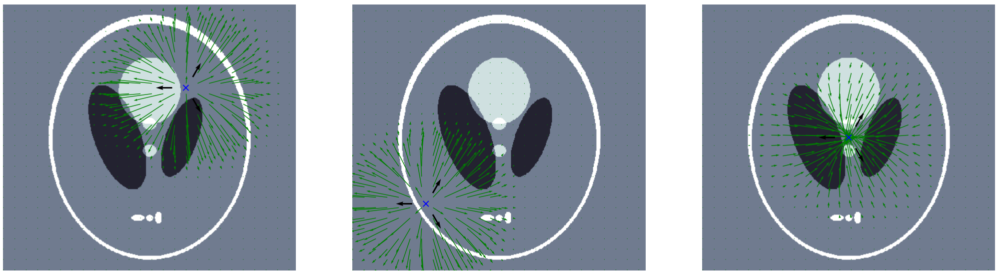

(a) Local scaling, $\sigma = 5$

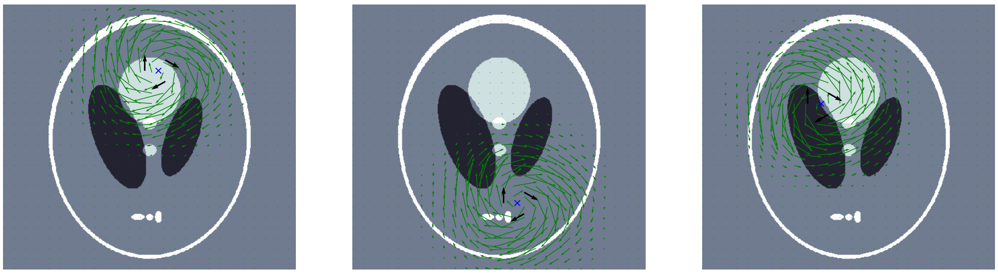

(b) Local rotation, $\sigma = 5$

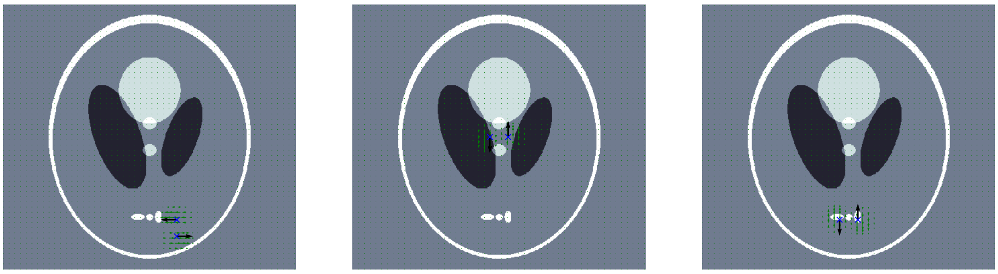

(c) Local shearing, $\sigma = 1.5$

Figure 4: Examples of vector fields generated by three constrained translations generator deformation modules (see Section 3.2.3) for three different choices of kernel-size σ, point-generator function f and vector-generator function g, leading to three types of vector fields: local scaling (Figure 4a), local rotation (Figure 4b) and local shearing (Figure 4c). For each deformation module, we present 3 examples of generated vector field for three different values of geometrical descriptors and controls. The blue crosses are the geometrical descriptors, vectors generated by the vector-generator functions g are in black (their base-points are points defined by $f(o)$) and the vector fields are plotted in green (the scalar controls are not represented, they are positive for left and middle figures, and negative for the right one).

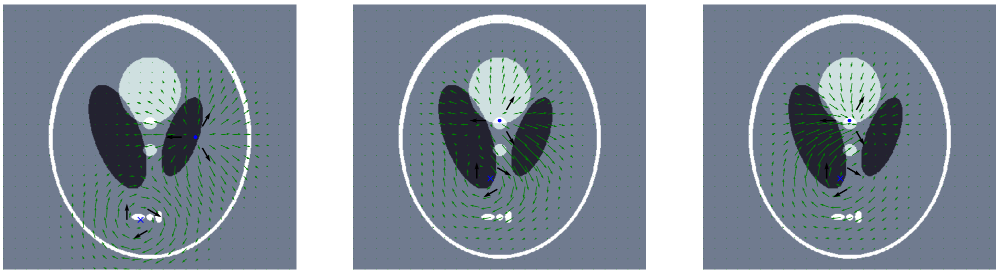

(a) Vector fields generated by combining a local rotation ($\sigma = 5$, geometrical descriptors are blue crosses) and a local scaling ($\sigma = 5$, geometrical descriptors are blue dots)

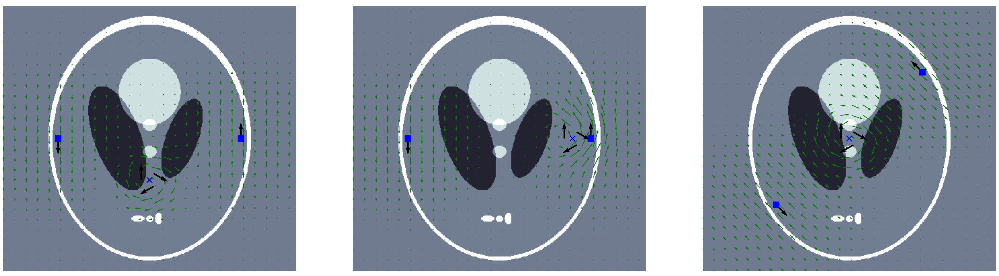

(b) Vector fields generated by combining a local rotation ($\sigma = 5$, geometrical descriptors are blue crosses) and a local shearing ($\sigma = 8$, geometrical descriptors are blue squares)

Figure 5: Examples of vector fields generated by two compound deformation modules. In Figure 5a are represented vector fields generated by combining deformation modules generating local scaling and local rotations. In Figure 5b are represented vector fields generated by combining deformation modules generating local shearing and local rotations. For each of the two compound deformation modules, we present 3 examples of generated vector field for three different values of geometrical descriptors and controls. The geometrical descriptors are plotted in blue, vectors generated by the vector-generator functions g are in black (their base-points are points defined by $f(o)$) and the vector fields in green (the scalar controls are not represented).

Definition 6. *Let $M = (\mathcal{O}, H, \zeta, c)$ be a deformation module and let a, b be in $\mathcal{O}$. We denote $\Theta_{a,b}$ the set of measurable curves $t \mapsto (o_t, h_t) \in \mathcal{O} \times H$ where o_t is absolutely continuous (a.c.), starting from a and ending at b, such that for almost every $t \in [0, 1]$, $\frac{\mathrm{d}}{\mathrm{d}t} o_t = v_t \cdot o_t$, where $v_t = \zeta_{o_t}(h_t)$, and*

$$E(o, h) = \int_0^1 c_{o_t}(h_t)\mathrm{d}t < \infty\,. \tag{3}$$

The quantity $E(o, h)$ is called the ***energy*** *of (o, h) and $\Theta_{a,b}$ is the set of* ***controlled paths of finite energy*** *starting at a and ending at b.*

In order to build constrained large deformations, it is necessary to show that the trajectory of vector fields $t \mapsto \zeta_{o_t}(h_t)$ defined from a controlled path of finite energy $t \mapsto (o_t, h_t)$ can be integrated in a trajectory of diffeomorphisms via the flow Equation (1). This is ensured by the following proposition, proved in [18].

Proposition 3. *Let us suppose that M satisfies UEC (with V the corresponding Hilbert space of vector fields). Let $(o, h) \in \Theta_{a,b}$ and for each t, $v_t = \zeta_{o_t}(h_t)$. Then $v \in L^2([0, 1], V) \subset L^1$, the flow φ^v exists, $h \in L^2([0, 1], H)$ and for each $t \in [0, 1]$, $o_t = \varphi^v_t.o_0$. We call the final diffeomorphism $\varphi^v_{t=1}$ (resp. the trajectory $t \mapsto \varphi^v_t$) a* ***modular large deformation generated by*** *a (resp. the* ***trajectory of modular large deformations generated by*** *(o, h)).*

Remark 5. *Such (constrained) modular large deformations will be used in Section 4 to transform a template image and perform constrained indirect registration.*

In Figure 6 we present an example of modular large deformation generated by the combination of two deformation modules. The first one generates "shearing" field at the scale $\sigma = 8$ its geometrical descriptors are formed of two points ($\mathcal{O} = \Omega \times \Omega$), the point-generator function is $f: o \mapsto o$ (identical function) and the vector-generator function is $g: o = (o_1, o_2) \in \Omega \times \Omega \mapsto (u^\perp, -u^\perp)$ where $u = o_1 - o_2 \in \mathbb{R}^2$ and, with $u = (u_x, u_y)$, $u^\perp = (u_y, -u_x)$ (vectors of $g(o)$ are orthogonal to the line between the two points of o). The second deformation module generates local rotations (at the scale $\sigma = 3$). We denote the compound deformation by $M^{\mathrm{CP}} = (\mathcal{O}^{\mathrm{CP}}, H^{\mathrm{CP}}, \zeta^{\mathrm{CP}}, c^{\mathrm{CP}})$ and the trajectory shown in Figure 6 is $\varphi^{\zeta^{\mathrm{CP}}_{o_t}(h_t)} \cdot I_0$ where $t \mapsto (o_t, h_t) \in \mathcal{O}^{\mathrm{CP}} \times H^{\mathrm{CP}}$ is a controlled path of finite energy (with h_t constant and positive), $t \mapsto \varphi^{\zeta^{\mathrm{CP}}_{o_t}(h_t)}$ the corresponding flow trajectory and I_0 an initial image.

This example illustrates that geometrical descriptors naturally follow the deformation of the ambient space during modular large trajectories due to the equation $\frac{\mathrm{d}}{\mathrm{d}t} o_t = \zeta_{o_t}(h_t) \cdot o_t$. We emphasize here that the geometrical descriptors of the two combined deformation modules are transported by the *total vector field generated by the compound deformation module*: in particular the centre of the rotation is displaced by the shearing field. Then, the area which is both rotated and translated by the shearing motion *remains the same during the whole trajectory.* Note that this is a direct consequence of the definition of the combination of deformation modules and that in order to build such deformations, one only needs to define two deformation modules and then apply the simple combination rule defined in Section 3.3.

3.5 Shooting equations

The goal of this article is to use the modular large deformations defined above in order to perform indirect registration. Let $M = (\mathcal{O}, H, \zeta, c)$ be a combination of CTG modules,

(a) $t = 0$ (b) $t = 0.25$ (c) $t = 0.5$ (d) $t = 0.75$ (e) $t = 1$

Figure 6: Deformation of the first image I_0 (at $t = 0$) by a trajectory of modular large deformation generated by the combination of two deformation modules. The corresponding geometrical descriptors are in blue (squares for shearing deformation module and cross for the rotation one) and vectors generated by the vector-generator functions g are in black.

with n the dimension of the ambient space and $\mathcal{O} \subset (\mathbb{R}^n)^m$ (see Section 3.3). We will not consider any modular large deformations that can be built from the deformation module M, but only these that minimize the energy (3) between starting and ending points. The corresponding trajectories (o, h) of geometrical descriptors and controls are called *geodesics*. In order to characterize such geodesics, we need to introduce the Hamiltonian $\mathcal{H}\colon (o, \eta, h) \in \mathcal{O} \times (\mathbb{R}^n)^m \times H \mapsto \sum_{i=1}^m \eta_i^T(\zeta_o(h)(o_i)) - \frac{1}{2}c_o(h)$ with $o = (o_1, \dots, o_m)$, $\eta = (\eta_1, \dots, \eta_m)$ and $\zeta_o(h)(o_i) \in \mathbb{R}^n$ the application of the vector field $\zeta_o(h)$ generated by (o, h) to the $i-$th point of o. As shown in [18], if (o, h) is a normal geodesics there exists $\eta\colon [0, 1] \mapsto (\mathbb{R}^n)^m$, called the *momentum* such that

$$\begin{cases} \frac{\mathrm{d}o_t}{\mathrm{d}t} &= \zeta_{o_t}(h_t^*) \cdot o_t \\ \frac{\mathrm{d}\eta_t}{\mathrm{d}t} &= -\partial_o \mathcal{H}(o_t, \eta_t, h_t^*) \\ h^* &= C_o^{-1} \sum_{k=1}^{n_H} \Big(\sum_{i=1}^m \eta_i^T(\zeta_o(e_k)(o_i)) \Big) e_k \, . \end{cases} \tag{4}$$

where $(e_1, \dots, e_{n_H})$ is a orthonormal basis of H and for each o in $\mathcal{O}$, the operator $C_o\colon H \mapsto H$ is defined by $(C_o h, h)_H = c_o(h)$ (with $(\cdot, \cdot)_H$ the inner product of H).

Proposition 4. *If the field generator ζ is at least C^2, the solution of this equation is totally defined by the initial conditions. Besides the solution $t \in [0, 1] \mapsto (o_t, \eta_t, h_t^*) \in \mathcal{O} \times (\mathbb{R}^n)^m \times H$ depends continuously on the initial conditions $(o_{t=0}, \eta_{t=0})$ when $C([0, 1], \mathcal{O} \times (\mathbb{R}^n)^m \times H)$ is equipped with the supremum norm.*

Proof. Indeed from Lemma 1(see below), the function $(o, \eta) \in \mathcal{O} \times (\mathbb{R}^n)^m \mapsto \Big(\zeta_{o_t}(h_t^*) \cdot o_t, -\partial_o \mathcal{H}(o_t, \eta_t, h_t^*)\Big)$ with $h^* = C_o^{-1}(\xi_o \circ \zeta_o)^*(\eta)$ is at least C^1 and then Equation (4) as a unique maximal solution for each initial condition in $\mathcal{O} \times (\mathbb{R}^n)^m$. The continuity of the solution with respect to the initial conditions can then be deduced from general theorems. □

Lemma 1. *If $M = (\mathcal{O}, H, \zeta, c)$ is a combination of L CTG modules (see Section 3.2.3), then for each o in $\mathcal{O}$, the operator C_o is invertible and $C^{-1}\colon o \in \mathcal{O} \mapsto C_o^{-1}$ is smooth.*

Proof. Let us denote $M^k = (\mathcal{O}^k, H^k, \zeta^k, c^k)$, $k = 1, \dots, L$ the CTG modules of which M is the combination. For each k, there exist functions f_i^k and g_i^k, $i = 1, \dots, p_k$ such that ζ^k is given by $\zeta^k\colon (o, h) \in \mathcal{O} \times H \mapsto h \sum_{i=1}^{p_k} K_\sigma(f_i^k(o), \cdot) g_i^k(o)$. From the definition of the cost one gets that for each k and for all (o, h) in $\mathcal{O}^k \times H^k$, $C_o^k(h) =$

$h(1 + \sum_{i,j} K_\sigma(f_i^k(o), f_j^k(o)) g_i^k(o)^T g_j^k(o))$ (let us recall that the control $h \in H^k$ is scalar). Since K_σ is a reproducing kernel, the quantity $\sum_{i,j} K_\sigma(f_i^k(o), f_j^k(o)) g_i^k(o)^T g_j^k(o)$ is always non-negative. As a consequence, the operator $C_o^{k^{-1}}$ is well defined for all o in $\mathcal{O}^k$ and from the smoothness of functions f_i^k and g_i^k on gets that $o \in \mathcal{O}^k \mapsto C_o^{k^{-1}} = \frac{1}{1+\sum_{i,j} K_\sigma(f_i^k(o), f_j^k(o)) g_i^k(o)^T g_j^k(o)}$ is smooth.

This is true for all k and as C_o is defined by $C_o \colon h = (h_1, \dots, h_L) \in H \mapsto \Big(C_{o_1}^1(h_1), \dots, C_{o_L}^L(h_L)\Big)$ for all $o = (o_1, \dots, o_L)$ in $\mathcal{O}$ (this is a direct consequence of the definition of the cost of a compound deformation module, see Section 3.3), it is clearly invertible and $o \mapsto C_o^{-1}$ is smooth. $\square$

Remark 6. *Using Proposition 4, in the following we will parametrize the modular deformations minimizing the energy by initial conditions in $\mathcal{O} \times (\mathbb{R}^n)^m$ (an initial geometrical descriptor and an initial momentum). The corresponding trajectory $t \mapsto (o_t, h_t)$ of geometrical descriptors and controls can be recovered by integrating Eq. (4) and then the modular large deformation is the flow (see Proposition 1) of the time-varying vector field $t \mapsto \zeta_{o_t}(h_t)$.*

4 Image reconstruction with a deformation prior

4.1 Constrained indirect registration

Let us consider $M = (\mathcal{O}, H, \zeta, c)$ a C^k-deformation module with $k \geq 2$, obtained by combining CTG modules, with $\mathbb{R}^n$ the ambient space and $\mathcal{O} = \Omega^M$ with $\Omega =]-\omega, \omega[^n$ for some ω in $\mathbb{R}$ (it is an open set of $\mathbb{R}^n$). The set Ω will be the set of $\mathbb{R}^n$ on which images are defined, and geometrical descriptors of $\mathcal{O}$ are formed of M points in Ω.

Let Y be a Banach space and D its distance. The idea here is to search, amongst all the modular large deformations parametrized by an initial variable in $\mathcal{O} \times (\mathbb{R}^n)^m$, the one allowing to perform the indirect registration between a given template in $L^2(\Omega, \mathbb{R})$ and some observed data in Y.

In all this section we set $T \colon L^2(\Omega, \mathbb{R}) \mapsto Y$ a continuous operator and $I_0 \in L^2(\Omega, \mathbb{R})$ a template image. Let $d \in Y$ be some data, the modular indirect registration between I_0 and d corresponds to minimizing:

$$J_d \colon (a, \eta_0) \in \mathcal{O} \times (\mathbb{R}^n)^m \mapsto \gamma R_1(a) + \tau R_2(\eta) + D\Big(T(\varphi_{t=1}^{\zeta_o(h)} \cdot I_0), d\Big)^2 \tag{5}$$

where (o, η) starts at $(o_{t=0}, \eta_{t=0}) = (a, \eta_0)$ and satisfies Equation (4), $\gamma, \tau \in \mathbb{R}_{>0}$, $R_1 \colon a \in \mathcal{O} \mapsto \sum_{x \in a} \frac{1}{||x|^2 - \omega^2|^2} \in \mathbb{R}_{>0} \cup \{\infty\}$ where the notation $\sum_{x \in a}$ means summation over all points which form the geometrical descriptor a, $R_2 \colon \eta \in (\mathbb{R}^n)^m \mapsto |\eta|^2 \in \mathbb{R}_{\geq 0}$.

Remark 7. *The regularization function R_1 takes finite values for geometrical descriptors $a \in \Omega^M$ such that the M points are in the open disc centred at zero with radius ω. Then it is assumed here that the initial geometrical descriptors should stay in this disc for the optimal solution. If this is too restrictive given the images (in particular if there should be some deformation occurring in the corners of the image), a simple solution is to extend the image (with value zero) on an extended domain $\tilde{\Omega} =]-2\omega, 2\omega[^n$ and to re-define $\mathcal{O}$ by $\tilde{\Omega}^M$ and R_1 by $a \in \mathcal{O} \mapsto \sum_{x \in a} \frac{1}{||x|^2 - (2\omega)^2|^2}$.*

Remark 8. *This reconstruction method consists in the minimization of Equation (5): it is an optimization problem on the space $\mathcal{O} \times (\mathbb{R}^n)^m$ which is of dimension $2nm$.*

4.2 Regularising properties

Proposition 5 (Existence)**.** *If the field generator ζ is at least C^2, for all d in Y, J_d has a minimizer in $\mathcal{O} \times (\mathbb{R}^n)^m$.*

Proof. Let $d \in Y$ and let us show that J_d has a minimizer in $\mathcal{O} \times (\mathbb{R}^n)^m$. Let $a_0 \in \mathcal{O}$, from the conditions on the regularization functions R_1 and R_2 and the fact that $\mathcal{O} \times (\mathbb{R}^n)^m$ is of finite dimension, there exists a compact set F of $\mathcal{O} \times (\mathbb{R}^n)^m$ such that for $(a, \eta) \in \mathcal{O} \times (\mathbb{R}^n)^m - F$, $J_d(a, \eta) > J_d(a_0, 0)$. We can assume that F contains $(a_0, 0)$. Then showing that J_d has a minimizer in $\mathcal{O} \times (\mathbb{R}^n)^m$ amounts to showing that it has a minimizer in F and, as F is compact, it is sufficient to check that J_d is continuous. First, from Proposition 4 and the continuity of ζ, we deduce that the trajectory of vector fields $t \in [0, 1] \mapsto \zeta_{o_t^{a,\eta_0}}(h_t^{a,\eta_0})$, where $(o^{a,\eta_0}, h^{a,\eta_0})$ is given by integrating Equation (4) with the initial condition (a, η_0), depends continuously on the initial conditions (a, η_0). As a consequence (see [12]), $(a, \eta_0) \mapsto \varphi_{t=1}^{\zeta_{o^{a,\eta_0}}(h^{a,\eta_0})} \cdot I_0 \in L^2(\Omega, \mathbb{R})$ is a continuous function which concludes the proof. □

Proposition 6 (Stability)**.** *Assume that the field generator ζ is at least C^2 and let d^k be a sequence of Y that converges to d in Y. For each k, let (a^k, η_0^k) be a minimizer of J_{d^k}. Then there exists a sub-sequence of (a^k, η_0^k) that converges to a minimizer of J_d.*

Proof. Let $a \in \mathcal{O}$, for each k, $J_{d^k}(a^k, \eta_k^0) \leq J_{d^k}(a, 0) = R_1(a) + R_2(0) + \frac{1}{\lambda} D(T(I_0), d_k)^2 \longrightarrow R_1(a) + R_2(0) + \frac{1}{\lambda} D(T(I_0), d)^2$. Then the sequences $R_1(a^k)$ and $R_2(\eta_0^k)$ are bounded and as a consequence (a^k, η_0^k) is in a compact set of $\mathcal{O} \times (\mathbb{R}^n)^m$ (because it is of finite dimension). Then up to an extraction, we can suppose that (a^k, η_0^k) converges to $(a^\infty, \eta_0^\infty)$ which leads to $J_{d^k}(a^k, \eta_0^k) \longrightarrow J_d(a^\infty, \eta_0^\infty)$ (because $d^k \longrightarrow d$ in Y). Then let (a, η_0) be in $\mathcal{O} \times (\mathbb{R}^n)^m$, for each k, $J_{d^k}(a^k, \eta_0^k) \leq J_{d^k}(a, \eta_0)$ so when taking the limit of both terms one gets $J_d(a^\infty, \eta_0^\infty) \leq J_d(a, \eta_0)$. This is true for any (a, η_0) so $(a^\infty, \eta_0^\infty)$ is a minimizer of J_d. □

Proposition 7 (Convergence)**.** *Assume that the field generator ζ is at least C^2 and let $d \in Y$. Assume that there exists $(\hat{a}, \hat{\eta}_0) \in \mathcal{O} \times (\mathbb{R}^n)^m$ such that $T(\varphi_{t=1}^{\zeta^{\hat{a},\hat{\eta}_0}} \cdot I_0) = d$ and $R_1(\hat{a}) < \infty$. Furthermore, assume that there exists a parameter selection rule $\gamma \colon \mathbb{R}_{>0} \mapsto \mathbb{R}_{>0}$, $\tau \colon \mathbb{R}_{>0} \mapsto \mathbb{R}_{>0}$ such that $\delta \mapsto \gamma(\delta)/\tau(\delta)$ and $\delta \mapsto \tau(\delta)/\gamma(\delta)$ are bounded and $\gamma(\delta) \to 0$, $\tau(\delta) \to 0$, $\delta^2/\gamma(\delta) \to 0$, $\delta^2/\tau(\delta) \to 0$ as $\delta \to 0$.*

Let (δ_k) be a sequence in $\mathbb{R}_{>0}$ converging to 0 and let (d_k) be a sequence in Y such that $D(d_k, d) \leq \delta_k$ for each k. Finally let, for each k, (a^k, η_0^k) be a minimizer of $J_{I_0, d^k, T}$. Then there exists a sub-sequence of (a^k, η_0^k) that converges to a minimizer of J_d in $\mathcal{O} \times (\mathbb{R}^n)^m$.

Proof. We set for each k, $\gamma_k = \gamma(\delta_k)$ and $\tau_k = \tau(\delta_k)$. Then, for each k we have:

$$\begin{aligned}
R_1(a^k) &\leq \tfrac{1}{\gamma_k} J_{d^k}(a^k, \eta_0^k) \leq \tfrac{1}{\gamma_k} J_{d^k}(\hat{a}, \hat{\eta}_0) \\
&= \tfrac{1}{\gamma_k} \Big(\gamma_k R_1(\hat{a}) + \tau_k R_2(\hat{\eta}_0) + D(T(\varphi_{t=1}^{\hat{a},\hat{\eta}_0} \cdot I_0), d_k)^2 \Big) \\
&\leq R_1(\hat{a}) + \tfrac{\tau_k}{\gamma_k} R_2(\hat{\eta}_0) + \tfrac{\delta_k^2}{\gamma_k}
\end{aligned}$$

From the hypothesis, we deduce that $R_1(a^k)$ is bounded and then that a_k is in a compact set. In a similar way we can show that η_0^k is in a compact set so up to an extraction we can suppose that (a^k, η_0^k) converges to $(a^\infty, \eta_0^\infty)$ in $\mathcal{O} \times (\mathbb{R}^n)^m$. As shown previously, this leads to

$$D(T(\varphi_{t=1}^{\zeta^{a^k,\eta_0^k}} \cdot I_0), d) \longrightarrow D(T(\varphi_{t=1}^{\zeta^{a^\infty,\eta_0^\infty}} \cdot I_0), d)\,.$$

Besides,

$$\begin{aligned} D(T(\varphi_{t=1}^{\zeta^{a^k,\eta_0^k}} \cdot I_0), d) &\leq D(T(\varphi_{t=1}^{\zeta^{a^k,\eta_0^k}} \cdot I_0), d^k) + D(d, d^k) \\ &\leq \sqrt{J_{d^k}(a_k, \eta_0^k)} + D(d, d^k) \\ &\leq \sqrt{\gamma_k R_1(\hat{a}) + \tau_k R_2(\hat{\eta}_0) + D(d, d_k)^2} + D(d, d^k) \end{aligned}$$

which tends to 0 for $k \longrightarrow \infty$. As a consequence:

$$D(T(\varphi_{t=1}^{\zeta^{a^\infty,\eta_0^\infty}} \cdot I_0), d) = 0$$

which concludes the proof. □

Remark 9. *We assume that $R_1(\hat{a}) < \infty$, if it is not the case it means that the boundary ω is not appropriate, in this case as explained previously, one only needs to increase it and extend the image.*

5 Application to image reconstruction

5.1 Overview

We present here examples of image reconstruction via modular indirect matching. In order to do so we minimize functional (5) with respect to the initial geometrical descriptor and momentum. Except in Section 5.3.2 the regularization parameters are $\tau = 10^{-5}$ and $\gamma = 10^{-5}$. The deformation modules that we use here are combinations of CTG modules (see Section 3.2.3). In all the experiments, the domain of the images is $\Omega = [-16, 16] \times [-16, 16]$ and is discretized using 256×256 pixels. We use the Operator Discretization Library (ODL) [1] in order to define discretized images (in particular for their interpolations) and operators. The optimisation is performed via a gradient descent, and the gradient is computed with a forward and backward integration scheme as described in [17] (Section 6), the algorithm is presented in Annexe A.

We present results of image reconstruction for two different types of operator T: a 2-D tomography operator and a restricting operator (they are defined in the corresponding sections). The data are in most cases noisy data, and we will specify the noise level by the signal-to-noise ratio (SNR), which is defined as

$$SNR(d) = 10 \log_{10}\left(\frac{\|d_0 - \overline{d_0}\|^2}{\|\epsilon - \overline{\epsilon}\|^2}\right),$$

where d_0 is the noise-free part of the data and $\epsilon = d - d_0$ the noise-part and $\overline{x}$ denotes the mean of x. The SNR is expressed in terms of decibel.

[1] https://github.com/odlgroup/odl

Remark 10. *In all the experiments, the initial geometrical descriptors are optimized. However, as we suppose that we know perfectly the deformation module to use, it is reasonable to assume also that we know approximately the location of the deformation. As a consequence we initialize the geometrical descriptors so that the location of the generated deformations are appropriate.*

5.2 2-D tomography operator

5.2.1 2-D tomography operator

In this example the forward operator T is the 2-D Ray transform defined by, for $I \in L^2(\Omega, \mathbb{R})$,

$$T(I)\colon (w, x) \in S^1 \times \mathbb{R}^2 \mapsto \int_{s \in \mathbb{R}, x+sw \in \Omega} I(x + sw) \mathrm{d}s \,,$$

where S^1 is the unit circle. In the discretized setting, we specify the angles (discretization of S^1) and the number of lines per angle (discretization of a bounded interval of $\mathbb{R}$). I used the implementation of the Ray transform of the Operator Discretization Library (ODL) [1]. In the first two examples (Sections 5.2.2 and 5.2.3), we use 100 angles uniformly distributed in $[0, \pi]$ and 724 lines per angle. In the last example we study the case of sparse and limited data.

5.2.2 Local rotation

We will first consider the same noise-free data as in Figure 1 for which unconstrained deformation frameworks do not give satisfying results. In order to obtain a better reconstructed image via constrained deformations, the prior to incorporate in the deformation model is that there should be an anisotropic rotation acting in the area of the small white structure. We present here an easy way to build a CTG module corresponding to this prior. We set the kernel size $\sigma = 0.5$, $\mathcal{O} = \Omega \times \Omega$ (geometrical descriptors are formed of two points) and we define f by associating, to each geometrical descriptor $o = (o_1, o_2)$, points regularly spaced by a distance σ in a rectangle grid of axis $o_1 - o_2$ (8 points in this direction) and its orthogonal (5 points in this direction, so that in total there are $8 \times 5 = 40$ points), see Figure 7. Then we define the function g so that the vector associated to $f_i(o)$ is $g_i(o) = R_{\frac{o_1+o_2}{2}, \frac{\pi}{2}}(f_i(o))$ where $R_{\frac{o_1+o_2}{2}, \frac{\pi}{2}}$ is the infinitesimal rotation (angle $\frac{\pi}{2}$) centred at $\frac{o_1+o_2}{2}$ (see Figure 7). In this example, the geometrical descriptors are made of $m = 2$ points so (see Remark 8 the dimension of the parameter to estimate is 8.

In Figure 8 we show the result of the indirect registration using this deformation module. We can see here that as we only allow the vector field at each time to be a local rotation, the desired deformations occurs. Then, if necessary, one could for instance study the estimated parameters of this deformation (given by the initial momentum).

5.2.3 Local rotation and additional deformation

Let us now consider the case where the ground truth is the image in Figure 9c and data are noisy (see Figure 9b, $SNR = 9.8$). In this case there are additional differences between the template and the ground truth. Let us suppose that the only prior that we have about the form of the deformation is that there are a “pushing-forces” acting (this can for instance model a growth) and that the area on which they act can be modelled via a Gaussian kernel. The easiest way to model this is via translations. We then build two deformation modules, each one generating one local translation. For each one the

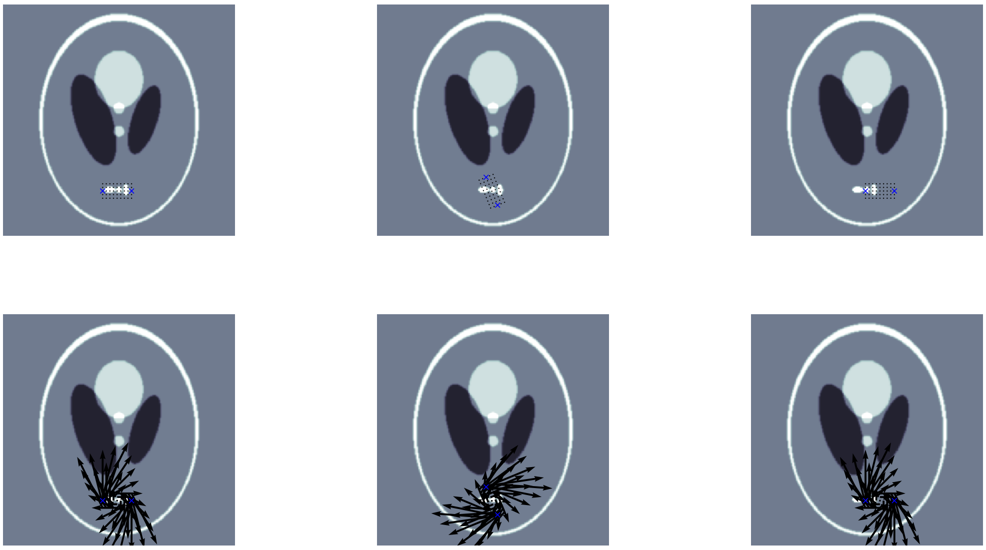

Figure 7: Examples of points $f(o)$ (first row, black points) and vectors $g(o)$ (second row, black vectors) generated by the deformation module presented in Section 5.2.2. Each column corresponds to an example of geometrical descriptor (in blue).

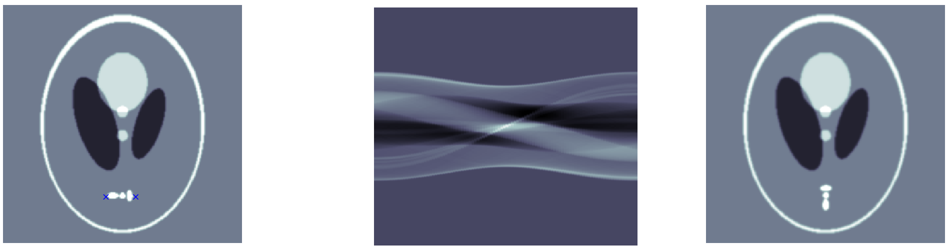

(a) Template. (b) Data. (c) Ground truth.

(d) $t = 0$. (e) $t = 0.25$. (f) $t = 0.5$. (g) $t = 0.75$. (h) $t = 1$.

Figure 8: Result of constrained indirect matching. Template I_0 in Figure 8a matched against data d in Figure 8b obtained from ground truth in Figure 8c (forward operator: Ray transform with 100 angles uniformly distributed in $[0, \pi]$) with the deformation module presented in Section 5.2.2. Second row: image trajectory $\varphi_t^{\zeta_o(h)} \cdot I_0$, the reconstructed image is then in Figure 8h. The blue crosses are the geometrical descriptors (their initialisation are in Figure 8a).

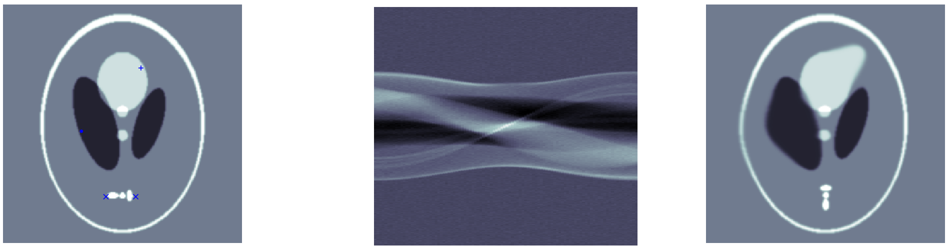

(a) Template. (b) Noisy data. (c) Ground truth.

(d) $t = 0$. (e) $t = 0.25$. (f) $t = 0.5$. (g) $t = 0.75$. (h) $t = 1$.

Figure 9: Result of constrained indirect matching. Template I_0 in Figure 9a matched against noisy data d in Figure 9b obtained from ground truth in Figure 9c (forward operator: Ray transform with 100 angles uniformly distributed in $[0, \pi]$) with the deformation module presented in Section 5.2.3. Second row: image trajectory $\varphi_t^{\zeta_o(h)} \cdot I_0$, the reconstructed image is then in Figure 9h. The geometrical descriptors are in blue (crosses for the anisotropic rotation, plus for the translation with $\sigma = 2$ and dot for the translation with $\sigma = 1$).

space of geometrical descriptors is then $\mathbb{R}^2$ (one point) and the space of controls is $\mathbb{R}^2$ (one vector). As previously (see Section 3.2.1) we use a Gaussian kernel, the kernel sizes are respectively 2 and 4 and are supposed to be known. We also use the previous deformation module generating a local and anisotropic rotation. Then we combine these three deformation modules (see Section 3.3). The result of the indirect registration using this compound deformation module is presented in Figure 9. In this example, the geometrical descriptors are made of $m = 4$ points so (see Remark 8 the dimension of the parameter to estimate is 16. As previously, the adapted rotation deformation is estimated by the gradient descent, and simultaneously the two translations "push" in the good direction to lead to a satisfying image reconstruction (Figure 9h).
This examples illustrates how one can easily complicate pre-existing deformation constraints (modelled by a given deformation module) by building new deformation modules and combining them with the pre-existing deformation module.

5.2.4 Limited and sparse data

One interest of our framework is that, by incorporating a deformation prior in the reconstruction method, we reduce the space of solutions and then good results can be obtained with limited data. We present here an example of this feature. We use the same template and ground truth image as in the previous Section 5.2.3 but data correspond to a discretized ray transform with 10 angles uniformly distributed in $[0.3\pi, 0.7\pi]$. This setting is more challenging than the previous one with full data and it is necessary to incorporate prior information in the reconstruction method in order to obtain satisfying results.

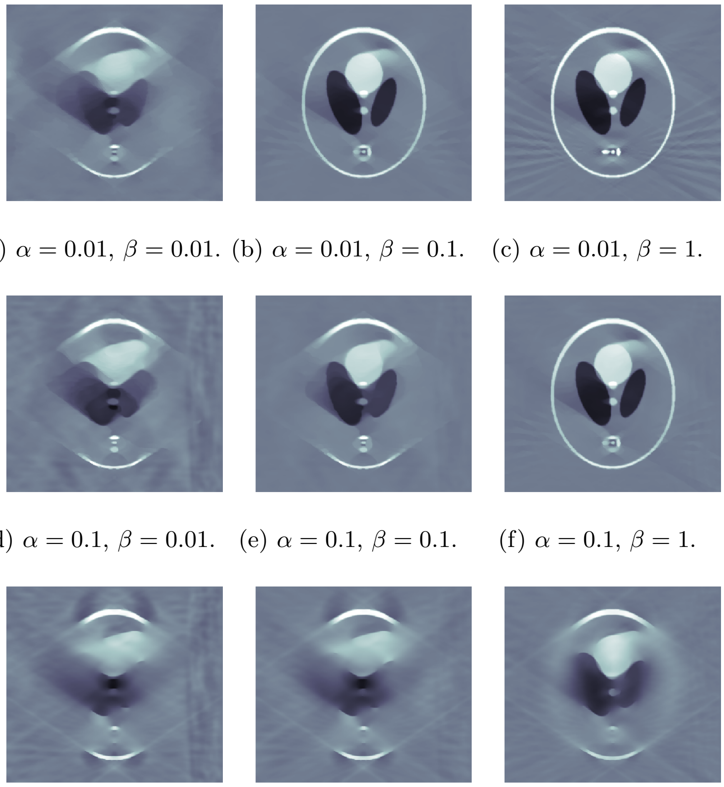

(a) $\alpha = 0.01$, $\beta = 0.01$. (b) $\alpha = 0.01$, $\beta = 0.1$. (c) $\alpha = 0.01$, $\beta = 1$.

(d) $\alpha = 0.1$, $\beta = 0.01$. (e) $\alpha = 0.1$, $\beta = 0.1$. (f) $\alpha = 0.1$, $\beta = 1$.

(g) $\alpha = 1$, $\beta = 0.01$. (h) $\alpha = 1$, $\beta = 0.1$. (i) $\alpha = 1$, $\beta = 1$.

Figure 10: Reconstruction with L^2-TV regularization in a sparse and limited angles setting (10 angles uniformly distributed in $[0.3\pi, 0.7\pi]$).

A classical way to use the template I_0 as a prior is to add a penalization of the L^2 distance to this template in the Total Variation (TV) algorithm. In this framework, the regularity of the solution I is controlled by $\alpha|\nabla I| + \beta|I - I_0|^2$ which depends on two regularization parameters α and β. We present on Figure 10 the results of this reconstruction method for different values of α and β. This shows that this method is not satisfying for this setting of limited and sparse angles.

On the contrary, as shown on Figure 11 our method gives good results for this setting.

5.3 Reconstruction from a partial observation

5.3.1 Framework and first example

We present now an example where the operator is a *restriction operator* which means that we only observe a small area of the whole image. This area will be a rectangle and then defined by its extremal points. This example illustrates how a prior knowledge about a 'large-scale motion' can allow to reconstruct an image from a 'small-scale observation'. The template, ground truth image and data are presented in Figure 14 (the observation window for the data is $[-5, 5] \times [-5, 5]$ and the SNR is 3). We suppose that we know that only two types of motions can happen here: an horizontal compressing motion (see Figure 12a) and a shearing motion (moving horizontally, see Figure 12b). A simple way to build a CTG module generating compressing (resp. shearing) vector field is to set $\mathcal{O} = \Omega \times \Omega$

(a) $t = 0$. (b) $t = 0.25$. (c) $t = 0.5$. (d) $t = 0.75$. (e) $t = 1$.

Figure 11: Result of constrained indirect matching in a sparse and limited angles setting (10 angles uniformly distributed in $[0.3\pi, 0.7\pi]$). This is the image trajectory $\varphi_t^{\zeta_o(h)} \cdot I_0$, the reconstructed image is then in Figure 11e.

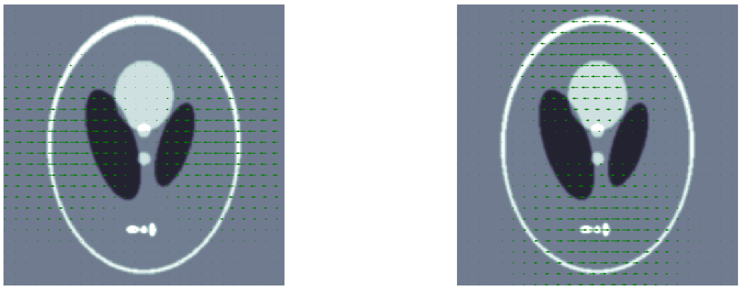

(a) Compressing motion. (b) Shearing motion.

Figure 12: Motions modelled in Section 5.3

(geometrical descriptors are made of two points), $f = Id_{\mathcal{O}}$ and $g\colon o = (o_1, o_2) \mapsto (u, -u)$ with $u = o_1 - o_2$ (resp. $g\colon o = (o_1, o_2) \mapsto (u^\perp, -u^\perp)$ with $u = o_1 - o_2 \in \mathbb{R}^2$ and, with $u = (u_x, u_y)$, $u^\perp = (u_y, -u_x)$). For these two deformation modules the kernel size is 8. See Figure 13 for illustrations of this construction.

The result of the indirect registration with the combination of these two deformation modules is presented in Figure 14. In this example, the geometrical descriptors are made of $m = 4$ points so (see Remark 8) the dimension of the parameter to estimate is 16. The image is well reconstructed: our method allows to understand how the whole image differs from the template one, even if only a small part is observed.

5.3.2 Robustness

We study here the robustness of our reconstruction method with respect to the regularization parameters, as well as the influence of the noise level on the reconstruction result.

Regularization parameters Our reconstruction methods relies on the minimization of the function (5) where two regularization parameters needs to be chosen: γ and τ. We launched the same experiment as in the previous Section 5.3.1 with different values for these parameters: $(1., 10^{-3}, 10^{-5}, 10^{-7})$ but fixed level of noise ($SNR = 3$). We show in Figure 15 the difference between the ground truth and our reconstructed image for each couple (γ, τ). We also give the value of the SSIM and the L^2 norm of this difference in

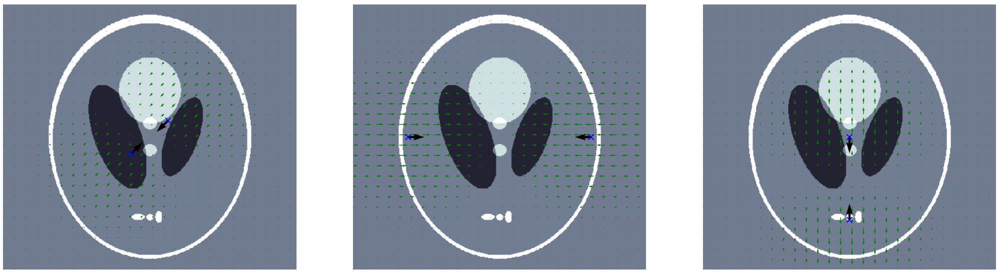

(a) Vector fields generated by deformation module generating compressing-dilating field. Geometrical descriptors are crosses.

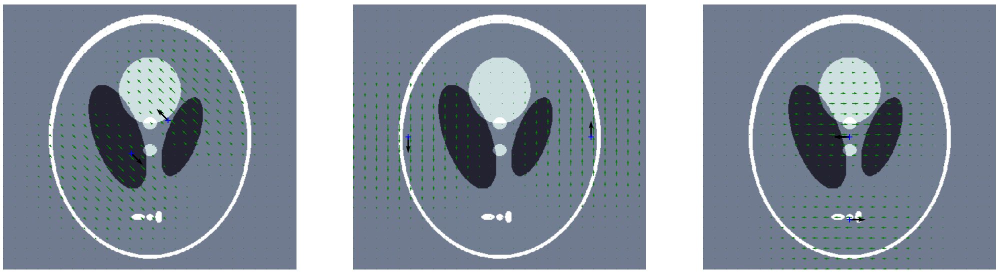

(b) Vector fields generated by deformation module generating shearing fields. Geometrical descriptors are pluses.

Figure 13: Examples of vector fields generated by the two deformation modules defined in Section 5.3 ($\sigma = 8$ for both). The geometrical descriptors o are plotted in blue, vectors $g(o)$ are in black and the vector fields in green (the scalar controls are not represented).

(a) Template.

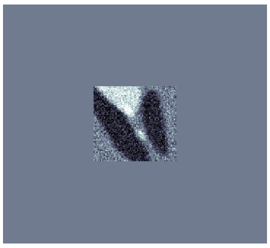

(b) Noisy data.

(c) Ground truth.

(d) $t = 0$.

(e) $t = 0.25$.

(f) $t = 0.5$.

(g) $t = 0.75$.

(h) $t = 1$.

Figure 14: Result of constrained indirect matching. Template I_0 in Figure 14a matched against noisy data d in Figure 14b obtained from ground truth in Figure 14c (forward operator: restricting operator) with the deformation module presented in Section 5.3. Second row: image trajectory $\varphi_t^{\zeta_o(h)} \cdot I_0$, the reconstructed image is then in Figure 14h. The geometrical descriptors are in blue (crosses for the compressing-field module and pluses for the shearing-field module.)

τ \ γ	1	10^{-3}	10^{-5}	10^{-7}
1	0.95	0.96	0.95	0.94
	1.98	1.58	2.05	2.17
10^{-3}	0.95	0.94	0.96	0.93
	1.97	2.24	1.72	2.62
10^{-5}	0.95	0.95	0.94	0.96
	2.05	1.90	2.15	1.78
10^{-7}	0.83	0.99	0.95	0.95
	5.28	0.65	1.93	2.12

Table 1: **SSIM** (top) and L^2 **difference with the ground truth** (bottom) values for various regularisation parameters.

SNR	10	3	0.04	-3
SSIM	0.99	0.98	0.92	0.91
L^2 difference	0.43	0.77	2.78	2.98

Table 2: **SSIM** and L^2 **difference with the ground truth** values for various noise level.

Table 1. Except for the extremal value $(\gamma, \tau) = (1, 10^{-7})$, all reconstructions are close to each other and satisfying.

Noise influence We present here the results for the same reconstruction problem as in Section 5.3.1 but for varying noise levels. In Figure 16 we show the difference between the reconstructed image and the ground truth, and in Table 2 we give the values of the SSIM and the L^2 norm of this difference.

5.3.3 Conclusion

The results of our regularization method on this example does not show a great sensitivity to the regularization parameter or the noise level. This is probably due to the fact that, by incorporating the deformation prior in the reconstruction method, we reduce the space of possible solutions.

6 Conclusion

We have presented a framework to reconstruct images as transformations of a known template image via constrained deformations. The deformations are constrained via CTG modules which are a particular category of deformation modules that is easy to use and can produce a wide variety of deformations. We showed that this is a well-defined regularization method, and illustrated that it allows to perform good reconstruction on 2-D simulated examples with noisy data. We showed in particular that incorporating deformation constraints enabled to recover a good reconstructed image from incomplete data: the prior compensates for the lack of data. In future works we intend to pursue in this direction: the idea is to use some motion prior, via the appropriate deformation modules,

(a) $\gamma = 1$, $\tau = 1$. (b) $\gamma = 1$, $\tau = 10^{-3}$. (c) $\gamma = 1$, $\tau = 10^{-5}$. (d) $\gamma = 1$, $\tau = 10^{-7}$.

(e) $\gamma = 10^{-3}$, $\tau = 1$. (f) $\gamma = 10^{-3}$, $\tau = 10^{-3}$. (g) $\gamma = 10^{-3}$, $\tau = 10^{-5}$. (h) $\gamma = 10^{-3}$, $\tau = 10^{-7}$.

(i) $\gamma = 10^{-5}$, $\tau = 1$. (j) $\gamma = 10^{-5}$, $\tau = 10^{-3}$. (k) $\gamma = 10^{-5}$, $\tau = 10^{-5}$. (l) $\gamma = 1^{-5}$, $\tau = 10^{-7}$.

(m) $\gamma = 10^{-7}$, $\tau = 1$. (n) $\gamma = 10^{-7}$, $\tau = 10^{-3}$. (o) $\gamma = 10^{-7}$, $\tau = 10^{-5}$. (p) $\gamma = 10^{-7}$, $\tau = 10^{-7}$.

Figure 15: Difference between reconstructed image and ground truth for several values of (γ, τ).

(a) $SNR = 10$. (b) $SNR = 3$. (c) $SNR = 0.04$. (d) $SNR = -3$.

Figure 16: Difference between reconstructed image and ground truth for several noise levels.

in order to efficiently reconstruct an image from temporal data when only few data are acquired at each time.

In all the numerical examples, we supposed that the appropriate deformation modules are perfectly known. In particular we suppose that the Gaussian kernel is an appropriate localizing function and that its kernel-size is known. This will in general not be the case with real data and we are currently working on methods to define the appropriate deformation modules, so that our reconstruction framework can be used easily with real data.

The final goal will be to estimate also the template image from temporal data so that we can perform full spatio-temporal reconstruction. In order to do so we will develop an iterative scheme where this image and the deformation are alternatively optimized.

As explained in Remark 1, the indirect registration framework is not satisfying when the grey-scale values of the template image are not correct. There would also be a problem with temporal data if a structure appears at a certain moment. In order to improve our reconstruction method, it will then be necessary to mix it with the metamorphosis framework.

7 Acknowledgements

The work by Barbara Gris was supported by the Swedish Foundation for Strategic Research grant AM13-0049.

A Algorithm

The algorithm that we computed and used to obtain the numerical results of Section 5 is available at [2]. It is implemented in a more generic context than the one presented here, in particular deformation modules that are not constrained translations generator ones can be used. Therefore we will not detail here the implementation, as it involves concepts and notation that are not introduced in this article. It is implemented in Python and relies on the class of objects DeformationModules. It uses the Operator Discretization Library (ODL) [3] in order to define discretized images and vector fields.

A.1 Deformation modules

An abstract class DeformationModule is defined with several functions, in particular the field generator ζ and the cost. CTG modules form a particular sub-class named TranslationBased. In the implementation we simplify slightly the definition of CTG module by defining the cost by $c\colon (o,h) \mapsto h^2$. Doing this we simplify the operator $C_o\colon H \mapsto H$ which becomes the Identity operator. Theoretically the UEC condition is no longer satisfied, this could lead to pathological trajectories such as non integrable time-varying vector fields. However, as long as the points forming the geometrical descriptors do not converge to each others during the minimization, the UEC condition is still satisfied because the norm of the generated vector field can be lower bounded with the norm of the control. As we do not observe such a convergence in practice, we can keep this simplified control.

[2] https://github.com/bgris/ConstrainedIndirectRegistration
[3] https://github.com/odlgroup/odl

A.2 Functional computation

The constrained indirect registration consists in the minimization of the functional (5) with respect to the initial geometrical descriptor $a \in \mathcal{O}$ and the initial momentum $\eta \in (\mathbb{R}^n)^m$. A first step is to compute this functional. As the computation of the regularization terms $(a, \eta_0) \in \mathcal{O} \times (\mathbb{R}^n)^m \mapsto \gamma R_1(a) + \tau R_2(\eta)$ is straightforward, we concentrate here on the computation of the attachment term $(a, \eta_0) \in \mathcal{O} \times (\mathbb{R}^n)^m \mapsto D(T(\varphi_{t=1}^{\zeta_o(h)} \cdot I_0, d)^2$ where D is the L^2 distance on the range of the operator T. The only difficult step here is to compute the transported image $\varphi_{t=1}^{\zeta_o(h)} \cdot I_0$. This is done by integrating (4) via an Euler scheme and transporting simultaneously the template image, see the sketch in Algorithm 1. In the particular case of a deformation module obtained by combination of CTG modules, the complexity of this forward integration is $O(Nmp^2)$ with m the total numbers of points forming the compound geometrical descriptor and p^2 the number of pixels of the image.

Algorithm 1 Computation of $\varphi_{t=1}^{\zeta_o(h)} \cdot I_0$.

Require: N ▷ time step for integration
Require: I_0 ▷ Initial template
Require: a, η_0 ▷ Initial geometrical descriptor and momentum
$I = I_0$, $o = a$, $\eta = \eta_0$ ▷ Initialization
for $i = 1, \dots, N$ **do**
  $h \leftarrow h^*$ ▷ See Equation (4)
  $\eta \leftarrow \eta - \frac{1}{N}\partial_o \mathcal{H}(o, \eta, h^*)$ ▷ See Equation (4)
  $v = \zeta_o(h^*)$
  $o \leftarrow o + \frac{1}{N} v \cdot o$
  $I \leftarrow I \circ (Id - \frac{1}{N} v)$
end for
return I

A.3 Gradient computation

As previously, the gradient of the regularization terms $(a, \eta_0) \in \mathcal{O} \times (\mathbb{R}^n)^m \mapsto \gamma R_1(a) + \tau R_2(\eta)$ is straightforward but the gradient of the attachment term $(a, \eta_0) \in \mathcal{O} \times (\mathbb{R}^n)^m \mapsto D(T(\varphi_{t=1}^{\zeta_o(h)} \cdot I_0, d)^2$ requires explanations. We use a *forward-backward* scheme based on the following result which is a simplified version of the more general principle (see for instance [3]):

Proposition 8. *Let $p \in \mathbb{N}$, $f \colon \mathbb{R}^p \mapsto \mathbb{R}^p$ a C^j vector field with $j \geq 1$ and $G \colon q_0 \in \mathbb{R}^p \mapsto S(q(t = 1))$ with $S \colon \mathbb{R}^p \mapsto \mathbb{R}$ C^1, $q \colon [0, 1] \mapsto \mathbb{R}^p$ defined by $q(t = 0) = q_0$ and*

$$\frac{\mathrm{d}}{\mathrm{d}t} q(t) = f(q(t)) \,. \tag{6}$$

Then for all $q_0 \in \mathbb{R}^p$, $\nabla G(q_0) = Z(0)$ where $Z \colon [0, 1] \mapsto \mathbb{R}^p$ is defined by $Z(1) = \nabla S(q(t = 1))$ and

$$\frac{\mathrm{d}}{\mathrm{d}t} Z(t) = \mathrm{d}f(q_t)^T Z(t) \tag{7}$$

This is called a *forward-backward scheme* because it consists in a forward step where Equation 6 is integrated, then the variable Z is initialized at $Z(1) = \nabla S(q(t = 1))$ and integrated backward following Equation 7. The computation of $\mathrm{d}f(q(t))^T$ can be quite hard in practice but it is shown in [3] that if $p = 2p_1$ and if there exists $\mathcal{H} \colon q \mapsto \mathbb{R}$

such that we can write for $q = (o, \eta) \in \mathbb{R}^{p_1} \times \mathbb{R}^{p_1}$, $f(q) = (\nabla_\eta \mathcal{H}(o, \eta), -\nabla_o \mathcal{H}(o, \eta))$, then for $Z = (Z_1, Z_2) \in \mathbb{R}^{p_1} \times \mathbb{R}^{p_1}$, $\mathrm{d}f(q(t))^T Z = \mathrm{d}\Big(\nabla \mathcal{H}\Big)(o, \eta) \cdot (-Z_2, Z_1)$ which can be approximated by finite differences.

We apply these results on a discretization of $\mathcal{O} \times (\mathbb{R}^n)^m \times L^2(\Omega, \mathbb{R})$, with the function f defined in the Algorithm 1. We are currently working on a new implementation of the gradient evaluation using automatic differentiation.

B Summary of notation

Notation	Signification
n	Dimension of the ambient space and the images (2 or 3)
$Diff_0^\ell(\Omega)$	Space of diffeomorphisms (see Section 2.3)
$C_0^\ell(\Omega, \mathbb{R}^n)$	Space of vector fields (see Section 2.3)
T	Forward operator
X	Space of images (reconstruction space)
Y	Data space
d	data
ϕ	Diffeomorphism
v	vector field
φ^v	Flow of v (see Equation (1))
K_σ	Scalar Gaussian kernel of scale σ (see Section 3.1)
M	Deformation module
$\mathcal{O}$	Space of geometrical descriptors
o	Geometrical descriptor
H	Space of controls
h	Control
h^*	Geodesic control (see Equation (4))
ζ	Field generator
c	Cost
η	Momentum (see Equation (4))

References

[1] I. Abraham, R. Abraham, M. Bergounioux, and G. Carlier. Tomographic reconstruction from a few views: a multi-marginal optimal transport approach. *Applied Mathematics & Optimization*, 75(1):55–73, 2017.

[2] Y. Amit, U. Grenander, and M. Piccioni. Structural image restoration through deformable templates. *Journal of the American Statistical Association*, 86(414):376–387, 1991.

[3] S. Arguillere. *Géométrie sous-riemannienne en dimension infinie et applications à l'analyse mathématique des formes*. PhD thesis, Paris 6, 2014.

[4] S. Arguillere, E. Trélat, A. Trouvé, and L. Younes. Shape deformation analysis from the optimal control viewpoint. *Journal de mathématiques pures et appliquées*, 2015.

[5] N. Aronszajn. Theory of reproducing kernels. *Transactions of the American mathematical society*, 68(3):337–404, 1950.

[6] V. Arsigny, O. Commowick, N. Ayache, and X. Pennec. A fast and log-euclidean polyaffine framework for locally linear registration. *Journal of Mathematical Imaging and Vision*, 33(2):222–238, 2009.

[7] V. Arsigny, X. Pennec, and N. Ayache. Polyrigid and polyaffine transformations: a novel geometrical tool to deal with non-rigid deformations–application to the registration of histological slices. *Medical image analysis*, 9(6):507–523, 2005.

[8] M. F. Beg, M. I. Miller, A. Trouvé, and L. Younes. Computing large deformation metric mappings via geodesic flows of diffeomorphisms. *International journal of computer vision*, 61(2):139–157, 2005.

[9] J.-D. Benamou, G. Carlier, M. Cuturi, L. Nenna, and G. Peyré. Iterative bregman projections for regularized transportation problems. *SIAM Journal on Scientific Computing*, 37(2):A1111–A1138, 2015.

[10] B. Berkels, A. Effland, and M. Rumpf. Time discrete geodesic paths in the space of images. *SIAM Journal on Imaging Sciences*, 8(3):1457–1488, 2015.

[11] M. Blume, A. Martinez-Moller, A. Keil, N. Navab, and M. Rafecas. Joint reconstruction of image and motion in gated positron emission tomography. *IEEE Transactions on Medical Imaging*, 29(11):1892–1906, 2010.

[12] M. Bruveris and D. D. Holm. Geometry of image registration: The diffeomorphism group and momentum maps. In *Geometry, Mechanics, and Dynamics*, pages 19–56. Springer, 2015.

[13] M. Burger, H. Dirks, L. Frerking, A. Hauptmann, T. Helin, and S. Siltanen. A variational reconstruction method for undersampled dynamic x-ray tomography based on physical motion models. *Inverse Problems*, 33(12):124008, 2017.

[14] C. Chen and O. Öktem. Indirect image registration with large diffeomorphic deformations. *SIAM Journal of Imaging Sciences*, 11(1):575–617, 2018.

[15] J. Ehrhardt, R. Werner, D. Säring, T. Frenzel, W. Lu, D. Low, and H. Handels. An optical flow based method for improved reconstruction of 4d ct data sets acquired during free breathing. *Medical Physics*, 34(2):711–721, 2007.

[16] U. Grenander, A. Srivastava, and S. Saini. A pattern-theoretic characterization of biological growth. *IEEE, Transactions on Medical Imaging*, 26(5):648–659, 2007.

[17] B. Gris. *Modular approach on shape spaces, Sub-Riemannian geometry and computational anatomy*. PhD thesis, Université Paris-Saclay, 2016.

[18] B. Gris, S. Durrleman, and A. Trouvé. A sub-riemannian modular framework for diffeomorphism based analysis of shape ensembles. 2016.

[19] B. Gris and O. Öktem. Image reconstruction through metamorphosis. 2018.

[20] E. Haber and J. Modersitzki. A multilevel method for image registration. *SIAM Journal on Scientific Computing*, 27(5):1594–1607, 2006.

[21] B. N. Hahn. Motion estimation and compensation strategies in dynamic computerized tomography. *Sensing and Imaging*, 18(1):10, 2017.

[22] J. Hinkle, M. Szegedi, B. Wang, B. Salter, and S. Joshi. 4d ct image reconstruction with diffeomorphic motion model. *Medical image analysis*, 16(6):1307–1316, 2012.

[23] A. Isola, A. Ziegler, T. Koehler, W. Niessen, and M. Grass. Motion-compensated iterative cone-beam ct image reconstruction with adapted blobs as basis functions. *Physics in Medicine & Biology*, 53(23):6777, 2008.

[24] J. Karlsson and A. Ringh. Generalized sinkhorn iterations for regularizing inverse problems using optimal mass transport. *SIAM Journal on Imaging Sciences*, 10(4):1935–1962, 2017.

[25] A. Katsevich. An accurate approximate algorithm for motion compensation in two-dimensional tomography. *Inverse Problems*, 26(6):065007, 2010.

[26] W. Lu and T. R. Mackie. Tomographic motion detection and correction directly in sinogram space. *Physics in Medicine & Biology*, 47(8):1267, 2002.

[27] B. A. Mair, D. R. Gilland, and J. Sun. Estimation of images and nonrigid deformations in gated emission ct. *IEEE Transactions on Medical Imaging*, 25(9):1130–1144, 2006.

[28] K. McLeod, M. Sermesant, P. Beerbaum, and X. Pennec. Spatio-temporal tensor decomposition of a polyaffine motion model for a better analysis of pathological left ventricular dynamics. *IEEE Transactions on Medical Imaging*, 34(7):1562–1575, 2015.

[29] J. Modersitzki. *Numerical methods for image registration.* Oxford University Press on Demand, 2004.

[30] S. Neumayer, J. Persch, and G. Steidl. Regularization of inverse problems via time discrete geodesics in image spaces. *arXiv preprint arXiv:1805.06362*, 2018.

[31] O. Oektem, C. Chen, N. O. Domanic, P. Ravikumar, and C. Bajaj. Shape-based image reconstruction using linearized deformations. *Inverse problems*, 33(3):035004, 2017.

[32] N. Portman. The modelling of biological growth: A pattern theoretic approach. 2010.

[33] M. Reyes, G. Malandain, P. M. Koulibaly, M. A. González-Ballester, and J. Darcourt. Model-based respiratory motion compensation for emission tomography image reconstruction. *Physics in Medicine & Biology*, 52(12):3579, 2007.

[34] S. Rit, J. Wolthaus, M. van Herk, and J.-J. Sonke. On-the-fly motion-compensated cone-beam ct using an a priori motion model. In *International Conference on Medical Image Computing and Computer-Assisted Intervention*, pages 729–736. Springer, 2008.

[35] C. J. Ritchie, J. Hsieh, M. F. Gard, J. D. Godwin, Y. Kim, and C. R. Crawford. Predictive respiratory gating: a new method to reduce motion artifacts on ct scans. *Radiology*, 190(3):847–852, 1994.

[36] M.-M. Rohé, N. Duchateau, M. Sermesant, and X. Pennec. Combination of polyaffine transformations and supervised learning for the automatic diagnosis of lv infarct. In *International Workshop on Statistical Atlases and Computational Models of the Heart*, pages 190–198. Springer, 2015.

[37] C. Seiler, X. Pennec, and M. Reyes. Capturing the multiscale anatomical shape variability with polyaffine transformation trees. *Medical image analysis*, 16(7):1371–1384, 2012.

[38] A. Srivastava, S. Saini, Z. Ding, and U. Grenander. Maximum-likelihood estimation of biological growth variables. In *Energy Minimization Methods in Computer Vision and Pattern Recognition*, pages 107–118. Springer, 2005.

[39] A. Trouvé and L. Younes. Metamorphoses through lie group action. *Foundations of Computational Mathematics*, 5(2):173–198, 2005.

[40] G. Van Eyndhoven, J. Sijbers, and J. Batenburg. Combined motion estimation and reconstruction in tomography. In *European Conference on Computer Vision*, pages 12–21. Springer, 2012.

[41] L. Younes. *Shapes and diffeomorphisms*, volume 171. Springer Science & Business Media, 2010.

[42] L. Younes. Constrained diffeomorphic shape evolution. *Foundations of Computational Mathematics*, 12(3):295–325, 2012.